Editors' Suggestion

Large quantum nonreciprocity in plasmons dragged by drifting electrons

Debasis Dutta* and Amit Agarwal†
Department of Physics, Indian Institute of Technology Kanpur, Kanpur-208016, India

(Received 14 December 2023; revised 22 May 2024; accepted 3 June 2024; published 2 July 2024)

Collective plasmon modes, riding on top of drifting electrons, acquire a fascinating nonreciprocal dispersion characterized by $\omega_p(\mathbf{q}) \neq \omega_p(-\mathbf{q})$. The classical plasmonic Doppler shift arises from the polarization of the Fermi surface due to the applied DC bias voltage. Here, we predict an additional quantum contribution to the plasmonic Doppler shift originating from the quantum metric of the Bloch wavefunction. We systematically compare the classical and quantum corrections to the Doppler shifts by investigating the drift-induced nonreciprocal plasmon dispersion in graphene and in twisted bilayer graphene. We show that the quantum plasmonic Doppler shift dominates in moiré systems at large wave vectors, yielding plasmonic nonreciprocity up to 20% in twisted bilayer graphene. Our findings highlight the significance of the quantum corrections to plasmonic Doppler shift in moiré systems and motivate the design of innovative nonreciprocal photonic devices with potential technological implications.

DOI: 10.1103/PhysRevB.110.045403

I. INTRODUCTION

Light propagates symmetrically in opposite directions in conventional optical systems. This is a consequence of the time-reversal invariance of Maxwell's equations or Lorentz's reciprocity principle [1–4]. Breaking reciprocity for asymmetric light propagation is conventionally done by magneto-optical approaches, which require large magnetic fields and limit the efficiency for nanoscale devices and on-chip integration [5]. To remedy this, nonreciprocal plasmonics in atomically thin two-dimensional (2D) materials, such as graphene, present opportunities for direction-dependent light propagation at the nanoscale. This is crucial for enabling compact devices in classical and quantum information processing, nonreciprocal devices for Faraday rotation, isolation, one-way waveguiding, and nonreciprocal cavities [6–8]. These make them a valuable addition to the nanophotonics toolbox [9–11].

Nonreciprocity in bulk plasmon dispersion can intrinsically arise in noncentrosymmetric magnetic materials. This is induced either by the dipolar distribution of the quantum metric or by the "chiral Berry" plasmons at the boundary of magnetic materials [12–15]. A more promising and controllable route for extrinsic breaking of Lorentz reciprocity is biasing the plasmonic material with a direct current. This induces nonreciprocal plasmons with a dispersion that differs for plasmons propagating along or opposite to the direction of the drifting carriers. This approach is minimally invasive for on-chip architectures, and it is known as the plasmonic Fizeau drag or Doppler effect [8,16–20]. Drift-induced nonreciprocal plasmons in single-layer graphene (SLG) have been recently predicted and demonstrated [16,18,20–23]. Using near-field imaging techniques, the plasmonic Doppler shift was measured for SLG [16,17] with a wavelength shift $\delta\lambda_p/\lambda_p \approx 2\%$ for electron drift velocity $u/v_F \approx 17\%$ (given $v_F = 0.86 \times 10^6$ m/s) [16]. These studies are primarily focused on the classical plasmonic Doppler shift, which primarily arises from the displacement of the Fermi surface due to drift flow (see Fig. 1) [16,18,20–23]. Additionally, the possibility of a quantum Doppler shift has been recently proposed in moiré systems owing to the band hybridization [19].

Motivated by these studies, we predict an exciting quantum Doppler shift-induced plasmonic nonreciprocity, which originates from the quantum metric—a band geometric property of the electron wavefunctions (see Fig. 1). Our investigation reveals that the classical correction varies linearly with the wave vector, while the quantum correction varies quadratically with the wave vector, as depicted in Fig. 1. We show that as flat band moiré systems have a large effective interaction strength and undamped plasmons at large wave vectors, twisted bilayer graphene (TBG) can support a large plasmonic nonreciprocity ($\sim$20%) driven by quantum correction. As a consequence, moiré materials in general and TBG in particular offers highly tunable platforms for observing and designing devices based on nonreciprocal light propagation [24–28].

II. NONRECIPROCAL PLASMONS WITH DC BIAS

The optical and plasmonic properties of a quantum system can be described by the dynamical density-density response function in the linear response of the applied electric field [29–31]. Plasmons are calculated from the zeros of the real part of the dielectric function. Within random-phase approximation (RPA), the dynamical dielectric function is calculated as [29,32,33]

$$\varepsilon(\mathbf{q}, \omega) = 1 - V_q \Pi(\mathbf{q}, \omega). \tag{1}$$

Here, $V_q = 2\pi e^2/(\kappa|\mathbf{q}|)$ denotes the 2D Fourier transform of the Coulomb potential, κ denotes an effective back-

*Contact author: ddebasis@iitk.ac.in
†Contact author: amitag@iitk.ac.in

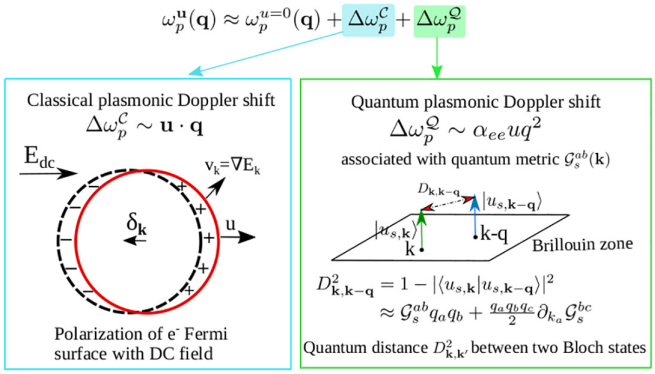

FIG. 1. The drift-induced nonreciprocal plasmon dispersion has both classical and quantum contributions. The classical frequency shift $\Delta\omega_p^{\mathcal{C}}$ arises from the polarization of the Fermi surface induced by the DC electric field. The solid and dashed lines represent the Fermi surface in the absence and presence of drift flow (u) of carriers. The quantum plasmonic Doppler shift, $\Delta\omega_p^{\mathcal{Q}}$, arises from the quantum metric $\mathcal{G}_s^{ab}(\mathbf{k})$ of the electron wavefunction in the presence of drifting charge carriers. The quantum metric is linked with the notion of quantum distance $D^2_{\mathbf{k},\mathbf{k}-\mathbf{q}}$ between two Bloch states at different momentum, $\mathbf{k}$ and $\mathbf{k}-\mathbf{q}$, respectively.

ground dielectric constant, and $\Pi(\mathbf{q},\omega)$ represents dynamical density-density response function [29,31,34].

We will treat the effect of externally applied DC current in a nonperturbative fashion by capturing its impact on the Fermi-Dirac distribution function [19,21,22]. In the hydrodynamic limit, we can model the drifting carrier distribution function as [16,35,36]

$$\tilde{f}_{s,\mathbf{k}} = \left\{\exp\left[\frac{E_{s,\mathbf{k}} - \mathbf{u}\cdot\mathbf{k} - \mu}{k_B T}\right] + 1\right\}^{-1}, \tag{2}$$

which nullifies the energy and momentum conserving electron-electron collision integral [35]. Here, $\mathbf{u}$ denotes the drift velocity of the quasiparticles, T denotes temperature, μ denotes the chemical potential, and $E_{s,\mathbf{k}}$ denotes Bloch band energy at crystal momentum $\mathbf{k}$ with band index s of the system. This drifting carrier distribution function induces a shift of the Fermi surface by momentum $\delta_{\mathbf{k}} = -m_{\text{eff}}\,\mathbf{u}$, in the small $u = |\mathbf{u}|$ limit [19] (see Sec. S1 of the Supplemental Material (SM) [37] for details). Here, m_{eff} denotes the effective mass of the quasiparticles.

Using this approach, we can express the DC current-driven noninteracting density-density response function for a 2D system as [21,29,39]

$$\Pi(\mathbf{q},\omega) = g_s \sum_{s,s'} \int \frac{d^2\mathbf{k}}{(2\pi)^2} \frac{(\tilde{f}_{s,\mathbf{k}+\mathbf{q}} - \tilde{f}_{s',\mathbf{k}}) F^{ss'}_{\mathbf{k}+\mathbf{q},\mathbf{k}}}{E_{s,\mathbf{k}+\mathbf{q}} - E_{s',\mathbf{k}} - \omega - i\eta}. \tag{3}$$

Here, $\tilde{f}_{s,\mathbf{k}}$ is the modified Fermi-Dirac distribution function at momentum $\mathbf{k}$ with band energies $E_{s,\mathbf{k}}$, g_s denotes the total degeneracy factor, and η is the broadening parameter. Here, the important quantity is the band coherence factor $F^{ss'}_{\mathbf{k}+\mathbf{q},\mathbf{k}} = |\langle u_{s,\mathbf{k}+\mathbf{q}}|u_{s',\mathbf{k}}\rangle|^2$, which describes the overlap between two energy eigenstates at momentum $\mathbf{k}$ and $\mathbf{k}+\mathbf{q}$. We set $\hbar = 1$ throughout our calculations and explicitly mention it when needed.

We first investigate the long-wavelength limit ($q \ll k_F$, where k_F denotes the Fermi wave vector) of the intraband plasmon dispersion in the presence of drift flow. For that, we expand the intraband band-overlap factor $F^{ss}_{\mathbf{k},\mathbf{k}+\mathbf{q}}$ up to $\mathcal{O}(q^3)$ [13,40], and obtain

$$F^{ss}_{\mathbf{k}\pm\mathbf{q},\mathbf{k}} \approx 1 - q_a q_b \mathcal{G}_s^{ab} \mp \frac{q_a q_b q_c}{2}\partial_{k_a}\mathcal{G}_s^{bc}. \tag{4}$$

Here, $\mathcal{G}_s^{ab}(\mathbf{k}) = [\text{Re}\langle\partial_{k_a}u_{s,\mathbf{k}}|\partial_{k_b}u_{s,\mathbf{k}}\rangle - \xi^a\xi^b]$ represents intraband quantum metric (or the Fubini-Study metric), with $\xi^a = i\langle u_{s,\mathbf{k}}|\partial_{k_a}u_{s,\mathbf{k}}\rangle$ being the single band Berry connection [13,24,41,42], and a, b, c denote cartesian directions. The quantum metric measures the distance between two infinitesimally close Bloch states in Hilbert space as [42,43] $D^2_{\mathbf{k},\mathbf{k}+d\mathbf{k}} = 1 - |\langle u_{s,\mathbf{k}}|u_{s,\mathbf{k}+d\mathbf{k}}\rangle|^2 \simeq \mathcal{G}_s^{ab}(\mathbf{k}) d\mathbf{k}^a d\mathbf{k}^b$.

We work in the dynamical long-wavelength limit, $qv_F < \omega \ll \mu$ (v_F denotes Fermi-velocity) to probe long-wavelength plasmons. In this limit, we expand the real part of the density-density response function in different orders of $1/\omega$. The calculation details are discussed in Sec. S2 of the SM. We obtain,

$$\text{Re}[\Pi_{\text{intra}}(\mathbf{q},\omega)] = q_a q_b q_c \frac{\mathcal{Q}^{\mathbf{u}}_{abc}}{\omega} + q_a q_b \frac{\mathcal{D}^{\mathbf{u}}_{ab}}{\omega^2} + q_a q_b q_c \frac{\mathcal{C}^{\mathbf{u}}_{abc}}{\omega^3} + \cdots. \tag{5}$$

We have used the $\mathbf{u}$ superscript to denote their drift current dependence. The expansion coefficients of Eq. (5) are specified by

$$\mathcal{Q}^{\mathbf{u}}_{abc} = -g_s \sum_{s,\mathbf{k}} \tilde{f}_{s,\mathbf{k}}\partial_{k_a}\mathcal{G}_s^{bc}(\mathbf{k}), \tag{6}$$

$$\mathcal{D}^{\mathbf{u}}_{ab} = g_s \sum_{s,\mathbf{k}} \tilde{f}_{s,\mathbf{k}}\left(\frac{\partial^2 E_{s,\mathbf{k}}}{\partial k_a \partial k_b}\right), \tag{7}$$

$$\mathcal{C}^{\mathbf{u}}_{abc} = 2g_s \sum_{s,\mathbf{k}} \tilde{f}_{s,\mathbf{k}}\left(v^a_{s,\mathbf{k}}\frac{\partial^2 E_{s,\mathbf{k}}}{\partial k_b \partial k_c}\right). \tag{8}$$

Here, $v^a_{s,\mathbf{k}} = \partial E_{s,\mathbf{k}}/\partial k_a$ represents the band velocity component. $\mathcal{Q}^{\mathbf{u}}_{abc}$ is the drift-induced quantum-metric dipole [13,25,41,44]. It is analogous to the Berry curvature dipole [45], with the Berry curvature [45] substituted by the quantum metric. In Eq. (7), $\mathcal{D}^{\mathbf{u}}_{ab}$ is the drift-renormalized Drude weight. In Eq. (8), $\mathcal{C}^{\mathbf{u}}_{abc}$ arises from the polarization of the Fermi-surface due to the momentum shift ($\delta_{\mathbf{k}}$) induced by the DC bias.

We find that the odd $1/\omega$ expansion coefficients in Eq. (6) and Eq. (8) are crucial for supporting nonreciprocal plasmons in the systems with $\Pi(\mathbf{q},\omega) \neq \Pi(-\mathbf{q},\omega)$. In the absence of drift, $\mathcal{Q}^{\mathbf{u}}_{abc}$ and $\mathcal{C}^{\mathbf{u}}_{abc}$ will be identically zero unless the system intrinsically breaks the inversion and time-reversal symmetry, simultaneously [13,15]. In that case, $\mathcal{Q}^{\mathbf{u}=0}_{abc}$, and $\mathcal{C}^{\mathbf{u}=0}_{abc}$ give rise to intrinsic nonreciprocal plasmon modes in noncentrosymmetric magnetic systems [13,15]. However, the unidirectional flow of drifting electrons breaks both the time-reversal and inversion symmetry, and it leads to an asymmetric Fermi-distribution function, $\tilde{f}_{s,\mathbf{k}} \neq \tilde{f}_{s,-\mathbf{k}}$. Therefore, the $\mathbf{k}$ integration of Eq. (6) and Eq. (8) are nonzero, yielding finite values of $\mathcal{Q}^{\mathbf{u}}_{abc}$ and $\mathcal{C}^{\mathbf{u}}_{abc}$ in the presence of finite u in all quantum systems.

We obtain the plasmon frequency by solving for the roots of Eq. (1) on the real axis [29], assuming the Landau damping to be relatively small. Retaining terms up to ω^3 in Eq. (5), we can approximate the long wavelength nonreciprocal plasmon dispersion. We calculate the drift-induced nonreciprocal plasmon dispersion for small q, up to linear order in u, to be (see Sec. S3 of the SM for details)

$$\omega_p^{\mathbf{u}}(\mathbf{q}) \approx \sqrt{q^2 V_q \mathcal{D}^{\mathbf{u}}} + \Delta\omega_p^{\mathcal{C}} + \Delta\omega_p^{\mathcal{Q}}\,. \tag{9}$$

Here, $\Delta\omega_p^{\mathcal{C}} = q\mathcal{C}^{\mathbf{u}}/2\mathcal{D}^{\mathbf{u}}$ captures the classical plasmon Doppler shift, and $\Delta\omega_p^{\mathcal{Q}} = q^3 V_q \mathcal{Q}^{\mathbf{u}}/2$ is the quantum plasmon Doppler shift.

Equation (9) captures the long-wavelength limit of nonreciprocal plasmon dispersion for general quantum systems with a DC current (retaining terms up to linear order in $\mathbf{u}$). Here, the first term captures the reciprocal plasmon dispersion with a drift velocity modified Drude weight, $\mathcal{D}^0 \to \mathcal{D}^{\mathbf{u}}$. Both of the other terms capture the nonreciprocal dispersion, as the sign of $\mathcal{Q}^{\mathbf{u}}$ and $\mathcal{C}^{\mathbf{u}}$ depends on whether the plasmon propagates along or opposite to the drift flow, i.e., $\hat{\mathbf{q}}\cdot\hat{\mathbf{u}} = \pm 1$. Of these two, the $\Delta\omega_p^{\mathcal{C}}$ term is a linear-in-q correction while the $\Delta\omega_p^{\mathcal{Q}}$ captures a quadratic correction to the nonreciprocal plasmon dispersion (for unscreened Coulomb interactions). The frequency shift $\Delta\omega_p^{\mathcal{C}}$ arises from the drift velocity induced shift of the Fermi surface, and it is typically referred to as classical correction or classical plasmonic Doppler shift [46]. In contrast, the second correction term $\Delta\omega_p^{\mathcal{Q}}$ in Eq. (9) has a completely quantum origin associated with the quantum-metric dipole $\mathcal{Q}^{\mathbf{u}}$. We term this correction as quantum plasmonic Doppler shift, as it arises from the nontrivial quantum geometry of the Bloch state [47]. This additional correction to the Doppler shift is one of the main findings of this manuscript. Interestingly, the quantum correction to the plasmonic Doppler shift can also be derived from a semiclassical hydrodynamic description. We present the semiclassical description of the plasmonic Doppler shift in Sec. 4 of the SM.

To quantify the classical and quantum nonreciprocity, we compute the percentage of nonreciprocity,

$$\frac{\left|\omega_p^{\mathbf{u}}(\mathbf{q}) - \omega_p^{\mathbf{u}}(-\mathbf{q})\right|}{\omega_p^0(\mathbf{q})} = \underbrace{\sqrt{q}\frac{\mathcal{C}^{\mathbf{u}}}{\mathcal{D}^{\mathbf{u}}}\sqrt{\frac{\kappa}{2\pi e^2 \mathcal{D}^0}}}_{\eta^{\mathcal{C}}} + \underbrace{q^{3/2}\mathcal{Q}^{\mathbf{u}}\sqrt{\frac{2\pi e^2}{\kappa\mathcal{D}^0}}}_{\eta^{\mathcal{Q}}}\,. \tag{10}$$

Here, $\eta^{\mathcal{C}}$ and $\eta^{\mathcal{Q}}$ denote the percentage of classical and quantum plasmonic nonreciprocity, respectively, and we have defined $\mathcal{D}^0 \equiv \mathcal{D}^{\mathbf{u}=0}$. Having established the origin of drift-induced quantum nonreciprocity, we next explore the magnitude of these terms in two-dimensional electron gas (2DEG), graphene, and twisted bilayer graphene.

III. QUANTUM NONRECIPROCITY IN GRAPHENE AND 2DEG

We calculate Eq. (9) for 2DEG with parabolic dispersion and graphene having linear dispersion to elucidate classical and quantum nonreciprocity. The wavefunction of a 2DEG is a single component object, and as a consequence, the band overlap term $F_{\mathbf{k},\mathbf{k}\pm\mathbf{q}} = 1$. This can also be seen from the fact that the Berry curvature and quantum metric vanish in single-component systems. Thus, a 2DEG can only support classical nonreciprocity with $\Delta\omega_p^{\mathcal{C}} = \mathbf{u}\cdot\mathbf{q}$, and the quantum contribution vanishes completely. We obtain the drift-induced plasmon dispersion for 2DEG from Eq. (9) to be

$$\omega_{\mathrm{2DEG}}^{\mathbf{u}}(\mathbf{q}) \approx \sqrt{\frac{2\pi n e^2}{\kappa m}q} + \mathbf{u}\cdot\mathbf{q}. \tag{11}$$

Here, n is the 2DEG carrier density and m is the effective mass. The detailed derivations are shown in Sec. S5 of the SM [37].

In contrast to 2DEG, the low energy electronic states for graphene is represented by 2D massless Dirac Hamiltonian, specified by $\mathcal{H}_{\mathbf{k}} = v_F\sigma\cdot\mathbf{k}$ with $\sigma = (\sigma_x, \sigma_y)$ being the vector of the Pauli matrices and v_F is the Fermi velocity [49]. This Hamiltonian has two component spinor eigenstates, $|\mathbf{k}, s\rangle = (1/\sqrt{2})(e^{-i\theta}\ \ s)^T$, with eigenvalues $E_{s,\mathbf{k}} = sv_F|\mathbf{k}|$ for conduction ($s = 1$) and valence ($s = -1$) band, respectively, and $\theta = \tan^{-1}(k_y/k_x)$. To understand the role of quantum geometry, we calculate the band resolved quantum metric, and it is given by $\mathcal{G}_+^{xx}(\mathbf{k}) = \mathcal{G}_-^{xx}(\mathbf{k}) = \sin^2\theta/(4k^2)$. The corresponding band overlap term can be evaluated using Eq. (4). For $\mathbf{q} = q\hat{\mathbf{x}}$, it is given by

$$F_{\mathbf{k}\pm\mathbf{q},\mathbf{k}}^{++} \approx 1 - \frac{q^2}{4k^2}\sin^2\theta \pm \cos\theta\sin^2\theta\frac{q^3}{2k^3}\,. \tag{12}$$

To include the impact of the unidirectional drift flow $\mathbf{u} = u\hat{\mathbf{x}}$ in the Fermi-Dirac distribution, we model it for $T = 0$ as $\tilde{f}_{+,\mathbf{k}} = \Theta[k_F(\theta) - k]$, where $k_F(\theta) = k_F/[1 - \beta\cos(\theta - \phi_u)]$. Here, $\beta = u/v_F$, and ϕ_u is the angle between $\mathbf{u}$ and plasmon wave vector $\mathbf{q}$. With this modified Fermi-distribution function, we can calculate the quantum metric dipole to be $\mathcal{Q}^{\mathbf{u}} = \gamma g_s u/(16\pi|\mu|)$. Here, $g_s = 4$ represents total spin and valley degeneracy, μ is the chemical potential, and $\gamma = \hat{\mathbf{q}}\cdot\hat{\mathbf{u}}$. For example, $\gamma = +1\,(-1)$ represents an up-stream (down-stream) plasmon propagation with respect to the drift of the charge carriers. We calculate the other expansion coefficients of $\Pi(\mathbf{q}, \omega)$ in Eq. (5) to be

$$\mathcal{D}^{\mathbf{u}} = \frac{g_s|\mu|}{4\pi}\frac{W(\beta)}{\beta}\,,\quad \mathcal{C}^{\mathbf{u}} = \gamma\frac{g_s v_F|\mu|}{8\pi}\frac{W(\beta)^2}{\beta}\,. \tag{13}$$

Here, we have defined $W(\beta) = 2(1 - \sqrt{1-\beta^2})/\beta$ and this relativistic factor becomes unity as $u \to 0$, or $\lim_{\beta\to 0} W(\beta)/\beta = 1$ [21]. Combining these terms, we calculate the long wavelength drift-induced nonreciprocal plasmon dispersion for graphene to be (see Sec. S6 of the SM [37] for detailed calculations)

$$\omega_p^{\mathbf{u}}(\mathbf{q}) \approx \sqrt{\frac{2D_0 W(\beta)}{\kappa\beta}}\sqrt{q}\left[1 + \frac{12 - 16\alpha_{\mathrm{ee}}^2}{16}\frac{q}{k_{\mathrm{TF}}}\right] + \gamma\frac{W(\beta)}{4\beta}uq + \gamma\frac{\alpha_{\mathrm{ee}}}{4k_F}uq^2. \tag{14}$$

Here, $D_0 = e^2\mu/\hbar^2$ is the noninteracting Drude weight at $T = 0$ for the 2D massless Dirac Hamiltonian [48], $\alpha_{\mathrm{ee}} = e^2/(\kappa\hbar v_F)$ is the effective-fine structure constant, and $k_{\mathrm{TF}} = 4\alpha_{\mathrm{ee}}k_F$ and κ is the background dielectric constant. In

TABLE I. The dependence of classical ($\eta^{\mathcal{C}}$) and quantum ($\eta^{\mathcal{Q}}$) percentage of plasmonic nonreciprocity for graphene on the wave vector, carrier density, and the effective-fine structure constant.

Graphene	$\eta^{\mathcal{C}} = \frac{\Delta\omega_p^{\mathcal{C}}(q)}{\omega_p^0(q)}$	$\eta^{\mathcal{Q}} = \frac{\Delta\omega_p^{\mathcal{Q}}(q)}{\omega_p^0(q)}$
Wave vector	$q^{1/2}$	$q^{3/2}$
Carrier density	$n^{-1/4}$	$n^{-3/4}$
Effective fine structure (α_{ee})	$\alpha_{ee}^{-1/2}$	$\alpha_{ee}^{1/2}$

Eq. (14), the last two nonreciprocal terms are calculated up to linear order in the drift velocity [16,21].

In Eq. (14), the classical Doppler shift due to $\mathcal{C}^u$ is $\Delta\omega_p^{\mathcal{C}} = \gamma[W(\beta)/4\beta]uq$, which arises from the polarization of the Fermi surface under DC field. Additionally, there is a quantum correction in Eq. (14) originating from the quantum-metric dipole $\mathcal{Q}^{\mathbf{u}}$, and this quantum Doppler shift is given by $\Delta\omega_p^{\mathcal{Q}} = \gamma(\alpha_{ee}/4k_F)uq^2$. This quantum correction goes as q^2 and varies with the carrier density as $n^{-1/2}$. We calculate the classical and quantum percentage of nonreciprocity in the plasmon dispersion to be

$$\eta^{\mathcal{C}} \equiv \frac{\Delta\omega_p^{\mathcal{C}}(q)}{\omega_p^0(q)} \sim \frac{1}{\alpha_{ee}}\frac{W(\beta)}{4\beta}\frac{u}{v_F}\frac{\omega_p^0(q)}{|\mu|}, \tag{15}$$

$$\eta^{\mathcal{Q}} \equiv \frac{\Delta\omega_p^{\mathcal{Q}}(q)}{\omega_p^0(q)} \sim \frac{u}{v_F}\frac{\omega_p^0(q)}{4|\mu|}\frac{q}{k_F}. \tag{16}$$

Here, $\omega_p^0(q) = |\mu|\sqrt{2\alpha_{ee}}(q/k_F)^{1/2}$ is the long-wavelength plasmon dispersion for graphene without drift flow [50]. We compare the dependence of both these corrections on different parameters such as wave vector, carrier density, and the interaction strength in Table I. We find that the quantum correction to the nonreciprocity is more sensitive to all these parameters. In Fig. 2(a), we present the total nonreciprocal plasmon dispersion in graphene for different drift velocities or

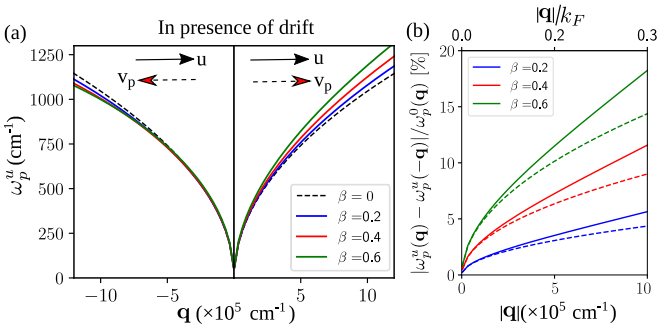

FIG. 2. (a) Plasmon dispersion for current-carrying graphene under different carrier drift velocities, $\beta = u/v_F = 0.2$, 0.4, and 0.6, respectively. Here, $v_p = d\omega_p/dq$ indicates the group velocity of plasmons. We have used $\alpha_{ee} = 0.9$ for air/SLG/SiO_2 interface [48] and carrier density, $n = 2.9 \times 10^{12}$ cm^{-2} [16]. (b) Total percentage of nonreciprocity $|\omega_p^u(\mathbf{q}) - \omega_p^u(-\mathbf{q})|/\omega_p^0(q)$ as a function of momentum ($\mathbf{q}$) for current-carrying graphene with different β. The dashed line represents the classical percentage of nonreciprocity ($\eta^{\mathcal{C}}$) as defined in Eq. (15). The horizontal q axis has been scaled in terms of the Fermi wave vector (k_F) at the top of panel (b). For SLG, the percentage of nonreciprocity is mainly dominated by classical contribution $\Delta\omega_p^{\mathcal{C}}$.

β. This includes both classical and quantum corrections. We also show the classical and total percentage of nonreciprocity separately in Fig. 2(b). For graphene, the total percentage of nonreciprocity is mainly dictated by the classical contribution with $\eta^{\mathcal{C}}$ [16]. The quantum correction is small in the range of experimentally accessible wave vectors. This is because the quantum correction $\Delta\omega_p^{\mathcal{Q}} \sim \alpha_{ee}uq^2$ is smaller for small wave vectors ($q < k_F$) with $\alpha_{ee} \approx 1$ [48]. The quantum correction can become significant for a larger wave vector ($q > k_F$), but the plasmon enters the particle-hole continuum region and becomes Landau damped [50]. This suggests that the quantum nonreciprocity of the plasmon dispersion can become larger in moiré superlattices of graphene, which support more significant $\alpha_{ee} \gg 1$ [19], and long-lived plasmon for larger wave vectors. Motivated by this, we investigate drift-induced nonreciprocal plasmon dispersion in the moiré superlattice of twisted bilayer graphene in the next section.

IV. LARGE PLASMONIC NONRECIPROCITY IN TWISTED BILAYER GRAPHENE

Moire superlattices, in general, and TBG, in particular, have attracted a lot of attention in near-field optical spectroscopy studies for probing novel collective plasmon modes [14,28,52]. Here, we specifically focus on the nature of drift-induced nonreciprocal plasmons in magic angle TBG.

The moiré superlattice has a large periodicity, of the order of tens of nanometers, for a small twist angle (θ). The real space lattice constant is specified by $L_M = a/[2\sin(\theta/2)]$, where $a \approx 0.246$ nm. This also leads to a smaller moiré Brillouin zone, with a reciprocal lattice vector of magnitude $k_M = k_{BG}\sin(\theta/2)$, with k_{BG} denoting the magnitude of the reciprocal lattice for bilayer-graphene (BG). Due to the interlayer electronic coupling and modulation of Dirac fermions by moiré superlattice potentials [51,53], the electronic band dispersion of small angle TBG shows distinct features compared to SLG and Bernal-stacked BG. Near magic angle $\theta \approx 1.05^\circ$, the low energy band structure of TBG has four quasiflat bands (two for valley, and two for spin degeneracy) with minimal bandwidth (∼8 meV) as shown in Fig. 3(a). The description of the continuum model Hamiltonian is discussed in Sec. S7 of the SM [37,54–58]. As a consequence, the effective Fermi velocity (v_{eff}) of the carriers close to the charge neutrality point becomes around $v_{eff} \sim 0.04v_F$, while SLG has $v_F = 0.86 \times 10^6$ m/s [see Fig. 3(b)]. As a consequence, the effective fine-structure constant in TBG, $\alpha_{ee} = e^2/(\kappa\hbar v_{eff})$, gets significantly enhanced ($\alpha_{ee} \sim 20 - 30$) compared to SLG having $\alpha_{ee} \approx 1$ [48]. We highlight this explicitly in Fig. 3(c) by showing the variation of α_{ee} in the first conduction band with doping.

To demonstrate the nonreciprocal plasmons in TBG, we have numerically calculated the loss-function spectrum, $L(\mathbf{q},\omega) = \mathrm{Im}[-\varepsilon^{-1}(\mathbf{q},\omega)]$ including all the intra ($s = s'$) and interband ($s \neq s'$) transitions for both K and K′ valleys. We present the calculated loss-function spectrum in pristine TBG (without drifting carriers) in Fig. 4(a). For our calculations, we have used 2D Coulomb potential $V_q = 2\pi e^2/(\kappa|\mathbf{q}|)$, with $\kappa = 4.9$ as the background static dielectric constant for hBN [59], and $T = 5$K. The loss function displays sharp peaks at the plasmon poles and shows the

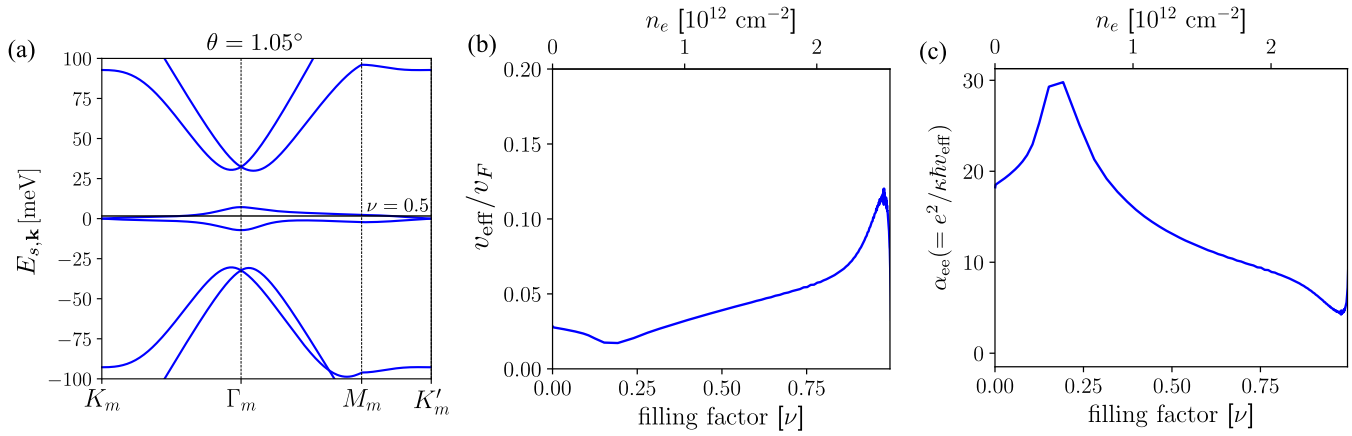

FIG. 3. (a) Band dispersion of twisted bilayer graphene near magic angle $\theta = 1.05^\circ$ for K valley only. We have used $u_0 = 79.7$ meV and $u_1 = 97.5$ meV in the continuum model [51]. The chemical potential is set at $\mu = 1.65$ meV, corresponding to half-filling. (b) The variation of effective Fermi-velocity ($v_{\rm eff}$) of TBG with charge filling factor ν in terms of Dirac fermion velocity ($v_F \approx 0.87 \times 10^6$ m/s) of single-layer graphene. Here, n_e denotes the corresponding carrier density. (c) Variation of the effective fine structure constant $\alpha_{\rm ee}$ for twisted bilayer graphene with filling factor. $\alpha_{\rm ee} > 10$ for a significant region of the band occupancy.

long-lived nature of the intraband plasmons in TBG in the terahertz frequency regime. In contrast to plasmons in SLG, the intraband plasmon mode in TBG lies above the Pauli blocking regions [$\omega_p^0(q) \gg 2\mu$] [28]. It becomes undamped from particle-hole excitations for large momentum as shown in Fig. 4(a). On applying a finite DC bias voltage and

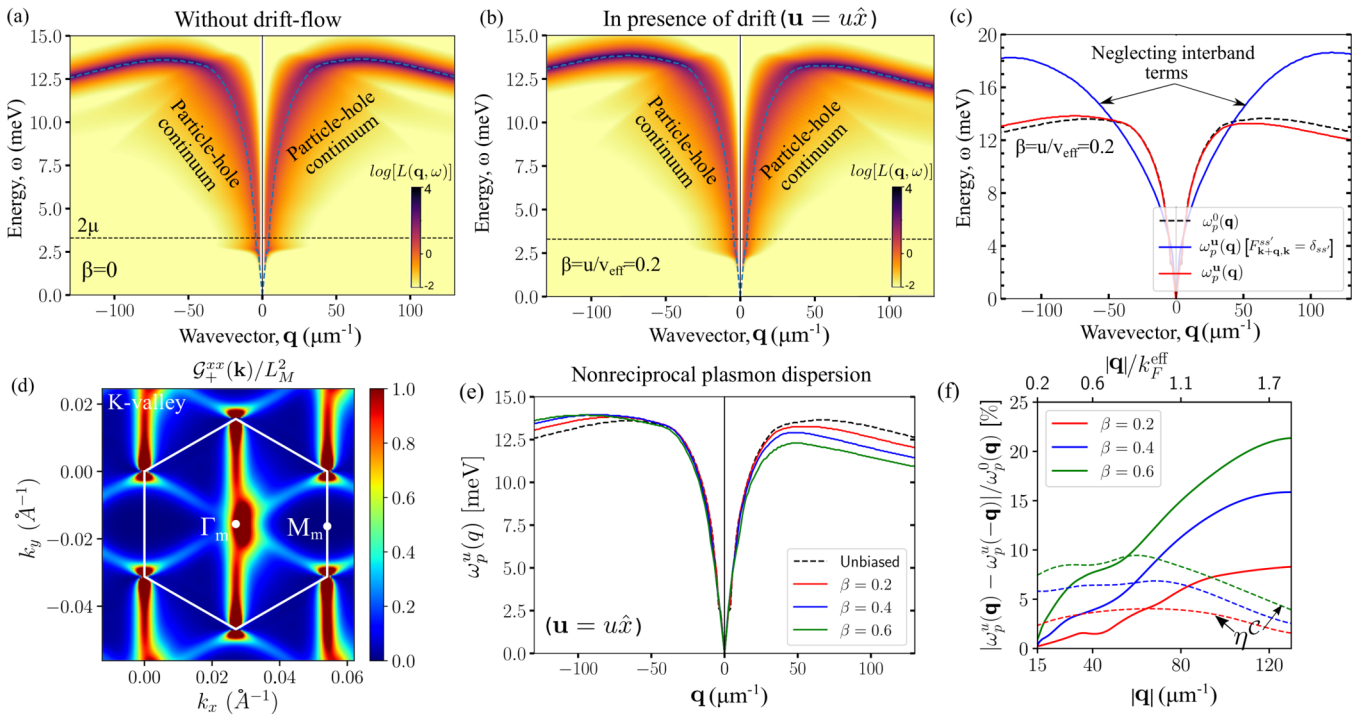

FIG. 4. (a) Colorplot of the loss function spectrum $L(\mathbf{q}, \omega) = \mathrm{Im}[-\varepsilon^{-1}(\mathbf{q}, \omega)]$ in log scale for twisted bilayer graphene (TBG) encapsulated in hBN (with $\kappa = 4.9$ [59]) at half-filling ($\mu = 1.65$ meV) without any DC bias. We set wave vector $\mathbf{q} \parallel \Gamma_m$-M$_{\rm m}$ direction as shown in panel (d). The cyan dashed line represents numerically evaluated plasmon dispersion by finding the roots of the dielectric function. (b) Loss function spectrum of biased TBG in the presence carriers drifting with velocity $\mathbf{u}$ along the x direction. The plasmon dispersion exhibits asymmetry for $+\mathbf{q}$ and $-\mathbf{q}$ wave vectors. (c) Nonreciprocal plasmon dispersion (shown by blue line) in TBG, without considering band geometric corrections by setting $F^{ss'}_{\mathbf{k}+\mathbf{q},\mathbf{k}} = \delta_{ss'}$. This neglects all interband contributions in the density-density response function. (d) Colormap of the quantum metri, $\mathcal{G}^{xx}_+(\mathbf{k})$ for the first conduction band in the K valley. (e) Nonreciprocal plasmon dispersion in TBG for different values of $\beta = u/v_{\rm eff} = 0.2$, 0.4, and 0.6, respectively. (f) Total percentage of nonreciprocity (solid lines) in TBG with different β. The horizontal axis at the top of the panel has been scaled in terms of the effective Fermi wave vector $k_F^{\rm eff} \approx 71\,\mu$m^{-1}. The dashed lines represent the classical percentage of nonreciprocity (η^C) with band-overlap factor $F^{ss'}_{\mathbf{k},\mathbf{k}\pm\mathbf{q}} = \delta_{ss'}$. Here, quantum corrections dominate over classical contributions, particularly in large wave vectors.

enabling drifting charge carriers in TBG, the Fermi surface shifts by momentum $\delta_{\mathbf{k}} = -\beta k_F^{\text{eff}} \hat{\mathbf{u}}$ where $\beta = u/v_{\text{eff}}$ and $v_{\text{eff}} = k_F^{\text{eff}}/m_{\text{eff}}$. Here, v_{eff} is the effective Fermi velocity, m_{eff} denotes the effective mass of the carriers, and $k_F^{\text{eff}} = \mu/(\hbar v_{\text{eff}})$ is the effective Fermi wave vector for TBG. We present the drift current (along the x direction) induced nonreciprocal loss function in the $\mathbf{q} - \omega$ plane in Fig. 4(b). The nonreciprocal nature of the plasmon dispersion with $\omega_p^{\mathbf{u}}(-\mathbf{q}) \neq \omega_p^{\mathbf{u}}(\mathbf{q})$ can be clearly seen. To investigate the classical correction in the nonreciprocity, we have calculated nonreciprocal dispersion in Fig. 4(c) by artificially setting the band-overlap factor, $F^{ss'}_{\mathbf{k},\mathbf{k}+\mathbf{q}} = \delta_{ss'}$, where $\delta_{ss'}$ denotes the Kronecker delta function. This approximation necessarily neglects all interband overlap terms, as well as band geometric corrections in TBG, mapping the TBG problem to a 2DEG case. The quantum corrections arise primarily from the quantum metric [see Eq. (6)], which dominates at larger wave vectors. This is because the plasmon mode is undamped in TBG for larger wave vectors, which allows to dominate $\Delta\omega_p^{\mathcal{Q}}(\mathbf{q})$ over $\Delta\omega_p^{\mathcal{C}}(\mathbf{q})$. We present the distribution of the quantum metric in the 2D Brillouin zone in Fig. 4(d).

Finally, we present the drift velocity dependence of the plasmon dispersion in Fig. 4(e) by numerically solving Eq. (1) for different ($\beta = u/v_{\text{eff}}$) values. We show the corresponding drift velocity dependence of the percentage of the plasmon nonreciprocity in Fig. 4(f). The classical correction overestimates the nonreciprocity for small q values. Interestingly, we find a significant increase in the percentage of total nonreciprocity between two oppositely propagating plasmon modes at larger wave vectors, driven predominantly by the quantum corrections [see Fig. 4(c)]. The quantum Doppler shift-induced plasmonic nonreciprocity can be more than 20% for $\beta \approx 0.6$. Furthermore, given the low value of v_{eff} in TBG, and in other moiré materials in general, achieving a more significant value of β in experiments should be feasible [60].

Our calculations strongly suggest that TBG and other moiré platforms with relatively flat bands can be good candidates to observe a significant quantum plasmonic Doppler effect. This is enabled by a rather large value of the effective interaction parameter ($\alpha_{\text{ee}} \propto 1/v_{\text{eff}}$) originating from the smaller band velocities in flat bands. It will be interesting to probe this large nonreciprocity in near-field imaging experiments [16,52]. Further, we note that all our calculations are within the RPA, which misses out on exchange and correlation effect [29]. Generally, RPA works very well for the plasmon dispersion. In fact, the plasmonic Doppler shift, calculated within RPA, explains the experimental dispersion for single-layer graphene reasonably well [17]. However, subtle effects in the plasmon nonreciprocity induced by exchange and correlation effects cannot be ruled out completely.

V. CONCLUSION

In summary, our investigation into drift-induced nonreciprocal plasmon dispersion in a general quantum system has unveiled an intriguing quantum plasmonic nonreciprocity alongside the well-established classical Doppler shift. The classical correction ($\Delta\omega_p^{\mathcal{C}}$) mainly arises from Fermi surface polarization under a DC electric field. In contrast, the quantum correction, ($\Delta\omega_p^{\mathcal{Q}}$), stems from the quantum-metric dipole—a fundamental band geometric property of the Bloch wave function.

Explicitly examining single-layer graphene and the moiré superlattice of twisted bilayer graphene, we observed distinct behaviors. In single-layer graphene, the classical term ($\Delta\omega_p^{\mathcal{C}} \sim uq$) predominantly governs the plasmonic Doppler shift, with the quantum correction ($\Delta\omega_p^{\mathcal{Q}} \sim \alpha_{\text{ee}} u q^2$) being relatively smaller owing to its q^2 behavior with $\alpha_{\text{ee}} \approx 1$ [48]. Conversely, the quantum metric-induced plasmonic quantum Doppler shift takes precedence in twisted bilayer graphene. This dominance arises from a small band velocity in the flat bands, resulting in a large effective fine structure constant ($\alpha_{\text{ee}} \approx 20 - 30$). Additionally, plasmons in twisted bilayer graphene remain practically undamped even for large values of q/k_F^{eff}, allowing the $\alpha_{\text{ee}} u q^2$ term in $\Delta\omega_p^{\mathcal{Q}}$ to influence the dispersion. Consequently, twisted bilayer graphene and other moiré systems can exhibit a plasmonic nonreciprocity of 20% or higher for reasonable drift velocities [60].

This exploration of drift-induced nonreciprocal plasmons in twisted bilayer graphene advances the fundamental understanding of the subject and paves the way for novel optoelectronic applications. Possibilities include the development of plasmonic isolators [61], one-way waveguides [62], and optical transmission [63].

ACKNOWLEDGMENTS

D.D. acknowledges the Indian Institute of Technology, Kanpur, for financial support. A.A. acknowledges the Department of Science and Technology for Project No. DST/NM/TUE/QM-6/2019(G)-IIT Kanpur, of the Government of India, for financial support. We thank Atasi Chakraborty and Debottam Mandal for the valuable discussions. We acknowledge the high-performance computing facility at IIT Kanpur for computational support. We also acknowledge the National Supercomputing Mission (NSM) for providing computing resources for "PARAM Sanganak" at IIT Kanpur.

[1] C. Caloz, A. Alù, S. Tretyakov, D. Sounas, K. Achouri, and Z.-L. Deck-Léger, Electromagnetic nonreciprocity, Phys. Rev. Appl. **10**, 047001 (2018).

[2] R. J. Potton, Reciprocity in optics, Rep. Prog. Phys. **67**, 717 (2004).

[3] S. V. Boriskina, M. Blevins, and S. Pajovic, The nonreciprocal adventures of light, Opt. Photon. News **33**, 46 (2022).

[4] Y. Tokura and N. Nagaosa, Nonreciprocal responses from non-centrosymmetric quantum materials, Nat. Commun. **9**, 3740 (2018).

[5] L. Bi, J. Hu, P. Jiang, D. H. Kim, G. F. Dionne, L. C. Kimerling, and C. A. Ross, On-chip optical isolation in monolithically integrated non-reciprocal optical resonators, Nat. Photonics **5**, 758 (2011).

[6] K. L. Tsakmakidis, L. Shen, S. A. Schulz, X. Zheng, J. Upham, X. Deng, H. Altug, A. F. Vakakis, and R. W. Boyd, Breaking lorentz reciprocity to overcome the time-bandwidth limit in physics and engineering, Science **356**, 1260 (2017).

[7] F. Monticone, A truly one-way lane for surface plasmon polaritons, Nat. Photonics **14**, 461 (2020).

[8] S. A. Hassani Gangaraj and F. Monticone, Drifting electrons: Nonreciprocal plasmonics and thermal photonics, ACS Photonics **9**, 806 (2022).

[9] D. N. Basov, M. M. Fogler, and F. J. G. de Abajo, Polaritons in van der waals materials, Science **354**, aag1992 (2016).

[10] A. Reserbat-Plantey, I. Epstein, I. Torre, A. T. Costa, P. A. D. Gonçalves, N. A. Mortensen, M. Polini, J. C. W. Song, N. M. R. Peres, and F. H. L. Koppens, Quantum nanophotonics in two-dimensional materials, ACS Photonics **8**, 85 (2021).

[11] C. Rizza, D. Dutta, B. Ghosh, F. Alessandro, C.-N. Kuo, C. S. Lue, L. S. Caputi, A. Bansil, V. Galdi, A. Agarwal, A. Politano, and A. Cupolillo, Extreme optical anisotropy in the type-II Dirac semimetal $NiTe_2$ for applications to nanophotonics, ACS Appl. Nano Mater. **5**, 18531 (2022).

[12] J. C. W. Song and M. S. Rudner, Chiral plasmons without magnetic field, Proc. Natl. Acad. Sci. USA **113**, 4658 (2016).

[13] A. Arora, M. S. Rudner, and J. C. W. Song, Quantum plasmonic nonreciprocity in parity-violating magnets, Nano Lett. **22**, 9351 (2022).

[14] T. Huang, X. Tu, C. Shen, B. Zheng, J. Wang, H. Wang, K. Khaliji, S. H. Park, Z. Liu, T. Yang, Z. Zhang, L. Shao, X. Li, T. Low, Y. Shi, and X. Wang, Observation of chiral and slow plasmons in twisted bilayer graphene, Nature (London) **605**, 63 (2022).

[15] D. Dutta, A. Chakraborty, and A. Agarwal, Intrinsic nonreciprocal bulk plasmons in noncentrosymmetric magnetic systems, Phys. Rev. B **107**, 165404 (2023).

[16] Y. Dong, L. Xiong, I. Y. Phinney, Z. Sun, R. Jing, A. S. McLeod, S. Zhang, S. Liu, F. L. Ruta, H. Gao, Z. Dong, R. Pan, J. H. Edgar, P. Jarillo-Herrero, L. S. Levitov, A. J. Millis, M. M. Fogler, D. A. Bandurin, and D. N. Basov, Fizeau drag in graphene plasmonics, Nature (London) **594**, 513 (2021).

[17] W. Zhao, S. Zhao, H. Li, S. Wang, S. Wang, M. I. B. Utama, S. Kahn, Y. Jiang, X. Xiao, S. Yoo, K. Watanabe, T. Taniguchi, A. Zettl, and F. Wang, Efficient fizeau drag from Dirac electrons in monolayer graphene, Nature (London) **594**, 517 (2021).

[18] D. S. Borgnia, T. V. Phan, and L. S. Levitov, Quasi-relativistic doppler effect and non-reciprocal plasmons in graphene, arXiv:1512.09044.

[19] M. Papaj and C. Lewandowski, Plasmonic nonreciprocity driven by band hybridization in moiré materials, Phys. Rev. Lett. **125**, 066801 (2020).

[20] T. A. Morgado and M. G. Silveirinha, Directional dependence of the plasmonic gain and nonreciprocity in drift-current biased graphene, Nanophotonics **11**, 4929 (2022).

[21] B. V. Duppen, A. Tomadin, A. N. Grigorenko, and M. Polini, Current-induced birefringent absorption and non-reciprocal plasmons in graphene, 2D Mater. **3**, 015011 (2016).

[22] M. Sabbaghi, H.-W. Lee, T. Stauber, and K. S. Kim, Drift-induced modifications to the dynamical polarization of graphene, Phys. Rev. B **92**, 195429 (2015).

[23] T. A. Morgado and M. G. Silveirinha, Nonlocal effects and enhanced nonreciprocity in current-driven graphene systems, Phys. Rev. B **102**, 075102 (2020).

[24] J. P. Provost and G. Vallee, Riemannian structure on manifolds of quantum states, Commun. Math. Phys. **76**, 289 (1980).

[25] A. Gao, Y.-F. Liu, J.-X. Qiu, B. Ghosh, T. V. Trevisan, Y. Onishi, C. Hu, T. Qian, H.-J. Tien, S.-W. Chen, M. Huang, D. Bérubé, H. Li, C. Tzschaschel, T. Dinh, Z. Sun, S.-C. Ho, S.-W. Lien, B. Singh, K. Watanabe, T. Taniguchi, D. C. Bell, H. Lin, T.-R. Chang, C. R. Du, A. Bansil, L. Fu, N. Ni, P. P. Orth, Q. Ma, and S.-Y. Xu, Quantum metric nonlinear Hall effect in a topological antiferromagnetic heterostructure, Science **381**, 181 (2023).

[26] J. Wang, J. Cano, A. J. Millis, Z. Liu, and B. Yang, Exact landau level description of geometry and interaction in a flatband, Phys. Rev. Lett. **127**, 246403 (2021).

[27] P. Bhalla, K. Das, D. Culcer, and A. Agarwal, Resonant second-harmonic generation as a probe of quantum geometry, Phys. Rev. Lett. **129**, 227401 (2022).

[28] C. Lewandowski and L. Levitov, Intrinsically undamped plasmon modes in narrow electron bands, Proc. Natl. Acad. Sci. USA **116**, 20869 (2019).

[29] G. Giuliani and G. Vignale, *Quantum Theory of the Electron Liquid*, Masters Series in Physics and Astronomy (Cambridge University Press, 2005).

[30] D. Pines and J. R. Schrieffer, Approach to equilibrium of electrons, plasmons, and phonons in quantum and classical plasmas, Phys. Rev. **125**, 804 (1962).

[31] D. Dutta, B. Ghosh, B. Singh, H. Lin, A. Politano, A. Bansil, and A. Agarwal, Collective plasmonic modes in the chiral multifold fermionic material cosi, Phys. Rev. B **105**, 165104 (2022).

[32] A. Agarwal, M. Polini, G. Vignale, and M. E. Flatté, Long-lived spin plasmons in a spin-polarized two-dimensional electron gas, Phys. Rev. B **90**, 155409 (2014).

[33] A. Agarwal and G. Vignale, Plasmons in spin-polarized graphene: A way to measure spin polarization, Phys. Rev. B **91**, 245407 (2015).

[34] R. Sachdeva, A. Thakur, G. Vignale, and A. Agarwal, Plasmon modes of a massive Dirac plasma, and their superlattices, Phys. Rev. B **91**, 205426 (2015).

[35] R. Bistritzer and A. H. MacDonald, Hydrodynamic theory of transport in doped graphene, Phys. Rev. B **80**, 085109 (2009).

[36] W. John, V. f. gantmakher, y. b. levinson. carrier scattering in metals and semiconductors. modern problems in condensed matter sciences vol. 19. north-holland: Amsterdam, oxford, new york, tokio 1987, 459 seiten. dfl. 280.00. isbn 0–444–87025–3, Cryst. Res. Technol. **23**, 230 (1988).

[37] See Supplemental Material at http://link.aps.org/supplemental/10.1103/PhysRevB.110.045403 for discusses, (i) Eq. (2) in different regimes, (ii) the density-density response function in small q limit, (iii) calculation of nonreciprocal plasmon dispersion, (iv) hydrodynamic theory of quantum plasmonic Doppler shift, (v) nonreciprocal plasmons in 2DEG, (vi) nonreciprocal plasmon dispersion in graphene, (vii) continuum model Hamiltonian for twisted bilayer graphene, and (viii) effective Fermi velocity in twisted bilayer graphene, and this also includes a Ref. [38].

[38] F. H. L. Koppens, D. E. Chang, and F. J. García de Abajo, Graphene plasmonics: A platform for strong Light–Matter interactions, Nano Lett. **11**, 3370 (2011).
[39] A. Agarwal, S. Chesi, T. Jungwirth, J. Sinova, G. Vignale, and M. Polini, Plasmon mass and drude weight in strongly spin-orbit-coupled two-dimensional electron gases, Phys. Rev. B **83**, 115135 (2011).
[40] E. Rossi, Quantum metric and correlated states in two-dimensional systems, Curr. Opin. Solid State Mater. Sci. **25**, 100952 (2021).
[41] Y. Gao and D. Xiao, Nonreciprocal directional dichroism induced by the quantum metric dipole, Phys. Rev. Lett. **122**, 227402 (2019).
[42] R. Resta, The insulating state of matter: A geometrical theory, Eur. Phys. J. B **79**, 121 (2011).
[43] A. Abouelkomsan, K. Yang, and E. J. Bergholtz, Quantum metric induced phases in moiré materials, Phys. Rev. Res. **5**, L012015 (2023).
[44] M. F. Lapa and T. L. Hughes, Semiclassical wave packet dynamics in nonuniform electric fields, Phys. Rev. B **99**, 121111(R) (2019).
[45] I. Sodemann and L. Fu, Quantum nonlinear Hall effect induced by berry curvature dipole in time-reversal invariant materials, Phys. Rev. Lett. **115**, 216806 (2015).
[46] H. Gao, Z. Dong, and L. Levitov, Plasmonic drag in a flowing Fermi liquid, arXiv:1912.13409.
[47] D. Xiao, M.-C. Chang, and Q. Niu, Berry phase effects on electronic properties, Rev. Mod. Phys. **82**, 1959 (2010).
[48] A. N. Grigorenko, M. Polini, and K. S. Novoselov, Graphene plasmonics, Nat. Photonics **6**, 749 (2012).
[49] A. H. Castro Neto, F. Guinea, N. M. R. Peres, K. S. Novoselov, and A. K. Geim, The electronic properties of graphene, Rev. Mod. Phys. **81**, 109 (2009).
[50] B. Wunsch, T. Stauber, F. Sols, and F. Guinea, Dynamical polarization of graphene at finite doping, New J. Phys. **8**, 318 (2006).
[51] M. Koshino, N. F. Q. Yuan, T. Koretsune, M. Ochi, K. Kuroki, and L. Fu, Maximally localized wannier orbitals and the extended hubbard model for twisted bilayer graphene, Phys. Rev. X **8**, 031087 (2018).
[52] N. C. H. Hesp, I. Torre, D. Rodan-Legrain, P. Novelli, Y. Cao, S. Carr, S. Fang, P. Stepanov, D. Barcons-Ruiz, H. Herzig Sheinfux, K. Watanabe, T. Taniguchi, D. K. Efetov, E. Kaxiras, P. Jarillo-Herrero, M. Polini, and F. H. L. Koppens, Observation of interband collective excitations in twisted bilayer graphene, Nat. Phys. **17**, 1162 (2021).
[53] R. Bistritzer and A. H. MacDonald, Moiré bands in twisted double-layer graphene, Proc. Natl. Acad. Sci. USA **108**, 12233 (2011).
[54] E. Y. Andrei and A. H. MacDonald, Graphene bilayers with a twist, Nat. Mater. **19**, 1265 (2020).
[55] J. M. B. Lopes dos Santos, N. M. R. Peres, and A. H. Castro Neto, Graphene bilayer with a twist: Electronic structure, Phys. Rev. Lett. **99**, 256802 (2007).
[56] A. Chakraborty, D. Dutta, and A. Agarwal, Tunable interband and intraband plasmons in twisted double bilayer graphene, Phys. Rev. B **106**, 155422 (2022).
[57] S. Sinha, P. C. Adak, A. Chakraborty, K. Das, K. Debnath, L. D. V. Sangani, K. Watanabe, T. Taniguchi, U. V. Waghmare, A. Agarwal, and M. M. Deshmukh, Berry curvature dipole senses topological transition in a moiré superlattice, Nat. Phys. **18**, 765 (2022).
[58] A. Chakraborty, K. Das, S. Sinha, P. C. Adak, M. M. Deshmukh, and A. Agarwal, Nonlinear anomalous Hall effects probe topological phase-transitions in twisted double bilayer graphene, 2D Mater. **9**, 045020 (2022).
[59] P. Novelli, I. Torre, F. H. L. Koppens, F. Taddei, and M. Polini, Optical and plasmonic properties of twisted bilayer graphene: Impact of interlayer tunneling asymmetry and ground-state charge inhomogeneity, Phys. Rev. B **102**, 125403 (2020).
[60] A. I. Berdyugin, N. Xin, H. Gao, S. Slizovskiy, Z. Dong, S. Bhattacharjee, P. Kumaravadivel, S. Xu, L. A. Ponomarenko, M. Holwill, D. A. Bandurin, M. Kim, Y. Cao, M. T. Greenaway, K. S. Novoselov, I. V. Grigorieva, K. Watanabe, T. Taniguchi, V. I. Fal'ko, L. S. Levitov, R. K. Kumar, and A. K. Geim, Out-of-equilibrium criticalities in graphene superlattices, Science **375**, 430 (2022).
[61] Z. Yu and S. Fan, Optical isolation based on nonreciprocal phase shift induced by interband photonic transitions, Appl. Phys. Lett. **94**, 171116 (2009).
[62] J. Yu, H. Chen, Y. Wu, and S. Liu, Magnetically manipulable perfect unidirectional absorber based on nonreciprocal magnetic surface plasmon, Europhys. Lett. **100**, 47007 (2012).
[63] A. B. Khanikaev, S. H. Mousavi, G. Shvets, and Y. S. Kivshar, One-way extraordinary optical transmission and nonreciprocal spoof plasmons, Phys. Rev. Lett. **105**, 126804 (2010).